Journal of Solid State Chemistry 335 (2024) 124700

Contents lists available at ScienceDirect

Journal of Solid State Chemistry

journal homepage: www.elsevier.com/locate/jssc

Synthesis of ultra-porous zeolitic imidazolate Framework-300 under different synthesis conditions for sorption of CO_2

Abolfazl Jomekian [a,*], Bahamin Bazooyar [b]

[a] Chemical Engineering Department, Esfarayen University of Technology, Esfarayen, Iran
[b] Center for Advanced Powertrain and Fuels, Brunel University London, Uxbridge, UB8 3PH, UK

ARTICLE INFO

Keywords:
ZIF-300
Precursors molar ratio
Temperature
Time
Synthesis environment

ABSTRACT

We examined here how different ratios of precursors, temperature, time, and synthesis environment affected the crystal structure, texture, and CO_2/N_2 sorption behavior of the ZIF-300 samples synthesized. We found that a higher bmim/meIm molar ratio resulted in larger particle size, increased pore volume, and higher BET surface area due to a more crystalline structure and well-shaped pore structure. This was attributed to a decrease in the pH of the synthesis solution caused by the higher bmim/meIm molar ratio, which lowered the ζ potential and reduced electrostatic repulsion between particles, leading to the formation of larger particles with a more crystalline structure. Increasing the temperature of the synthesis solution resulted in smaller particles due to a decrease in supersaturation levels and the formation of smaller nuclei. The duration of synthesis had a positive effect on particle size as both growth and aggregation of smaller particles occurred over time. NMP and DMA were found to be unsuitable synthesis environments as they produced large particles with poor gas sorption performance. In terms of texture, ZIF-300 samples synthesized with a higher bmim/meIm molar ratio and at lower temperatures exhibited higher BET surface area and pore volume compared to other samples. Additionally, samples synthesized with a molar ratio of bmim/meIm = 4/1 and 2/1 showed better selectivity for CO_2/N_2 solubility compared to similar cases reported in previous studies.

1. Introduction

The worldwide rate of fossil fuel consumption in recent years has increased sustrationally and it is expected that we experience another 50% increase in less than 30 years [1]. The main effect of this increased fossil fuel consumption will be the tremendous increase in the emission of global warming gases such as CH_4, CO, NO_x and mostly CO_2 in the atmosphere [2]. Currently, global warming is a crisis worldwide and its effect on human life is being felt in different parts of the world by observation of more destructive and unprecedented thunderstorms, floods, heat waves, constant rain, droughts, sea level rise, etc [3]. This means that the current rate and trend of producing global warming gases is a threat to a sustainable future generation life. The main part of global warming gas consists of CO_2, which is produced in almost every human activity related to the consumption of energy sources [4]. Therefore it is essential to look for methods of reducing CO_2 production and emission in the atmosphere. One approach is to separate CO_2 from other gases and prevent it from entering the environment and it is called the carbon capture process [5]. CO_2 absorption by solvents [6,7], cryogenic operations [8,9], membrane processes, and adsorption [10,11] are the most renowned methods of carbon capture. Adsorption is one of the most promising and cost-effective methods applied in experimental and industrial scales for CO_2 capture. The main requirement of this method is the availability or synthesis of an effective adsorbent. One of the promising and most effective types of adsorbents for CO_2 capture is metal-organic frameworks (MOFs) [12]. In these adsorbents, different types of inorganic and organic linkers form a 3D structure with unique pore size and functionality which is an advantage of these materials compared with many inorganic and organic porous materials [13–16]. One of the renowned subfamily of MOFs is called zeolitic imidazolate frameworks (ZIFs) in which a tetrahedral coordination was formed from the link of CO or Zn with imidazole derivatives. ZIFs showed the advantages of high specific surface area, high pore volume, and controllable and flexible pore channels with the ability to be easily functionalized [17,18]. This makes them very interesting to be used in CO_2 adsorption applications. These materials can adsorb CO_2 nearly 83 times their volume [19]. Among various and numerous types of ZIFs structures that have been reported in the literature, only a few

* Corresponding author.
E-mail addresses: a.jomekian@esfarayen.ac.ir (A. Jomekian), B.bazooyar@brunel.ac.uk (B. Bazooyar).

https://doi.org/10.1016/j.jssc.2024.124700
Received 28 January 2024; Received in revised form 21 March 2024; Accepted 30 March 2024
Available online 1 April 2024

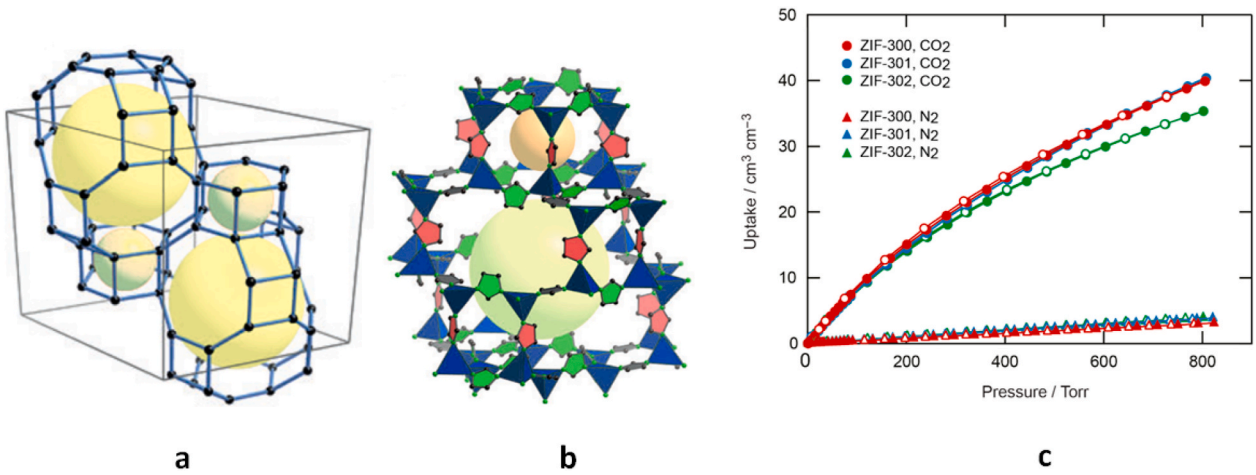

Fig. 1. a) Cha-net showed by ball and stick model [20], b) Crosslinked cha (large) and hpr (small) cages [20] and c) the CO_2 and N_2 adsorption isotherms of ZIF-300, ZIF-301 and ZIF-302 samples at 298 K [20].

Table 1
The used alias of different synthesized ZIF-300 samples along with their synthesis conditions.

Code name of ZIF-300 sample	bmim (mmol)	meIm (mmol)	$Zn(NO_3)_2.6H_2O$	Solvent type	Temperature of synthesis environment
ZIF-300–1/4	1.43	5.72	1.14	DMF	120 °C
ZIF-300–1/2	1.43	2.86	1.14	DMF	120 °C
ZIF-300–1/1 or (ZIF-300–120)or (ZIF-300-DMF)	1.43	1.43	1.14	DMF	120 °C
ZIF-300–2/1	2.86	1.43	1.14	DMF	120 °C
ZIF-300–4/1	5.72	1.43	1.14	DMF	120 °C
ZIF-300–80	1.43	1.43	1.14	DMF	80 °C
ZIF-300–100	1.43	1.43	1.14	DMF	100 °C
ZIF-300–140	1.43	1.43	1.14	DMF	140 °C
ZIF-300-DMA	1.43	1.43	1.14	DMA	120 °C
ZIF-300-NMP	1.43	1.43	1.14	NMP	120 °C

topologies have been considered to be effective in sorption applications. In recent years, the Yaghi group demonstrated that a rare ZIF topology also can be relatively easily formed in synthesis procedure of ZIF-300, ZIF-301 and ZIF-302 with mixed-link approach [20]. In these ZIF materials, zinc atoms in a tetrahedral arrangement are enclosed by four double-bonded imidazolate connections and connected by imidazolate bridges to form a three-dimensional CHA structure [20]. The CHA topology consists of four distinct crystallographic edges. (Fig. 1a).

Upon detailed analysis of the crystal structures reported by Yaghi et al. [20], it was observed that in all cases, the 2-mIm links are consistently located at the edge connecting the two 6-membered rings that generate the (hpr) cage. Furthermore, the substituted bIm links have specific positions within the (cha) cages that do not share edges with the (hpr) cages (Fig. 1b). The other two edges which are shared by the hpr and cha cages, do not show a specific preference for either 2-mIm or the substituted bmim in ZIF-300. Among repoted three types of ZIF materials (ZIF-300, ZIF-301 and ZIF-302), ZIF-300 demonstrated significantly higher and the best CO_2 sorption capacity and longer lifespan compared with the its two other counterparts (Fig. 1c). There are a few studies on CO_2 separation performance of this material in the form of mixed matrix membrane since their invention. Yuan et al. [21] synthesized ZIF-300/PEBA mixed matrix membrane for CO_2/N_2 separation and their best performing sample surpassed CO_2/N_2 Robeson upper bond of 2008. Sarfraz and Shammakh [22] synthesized an integrated ZIF-300/GO/Ultrason membrane for CO_2/N_2 separation. They observed significant improvement in both CO_2 permeability and CO_2/N_2 selectivity (nearly three times higher) compared with pure Ultrason membrane. From investigating the literature, it can be concluded that there is series lack of comprehensive studies on structure, modification and sorption and separation properties of ZIF-300 material which showed high potential to be used as CO_2 adsorbent. Therefore, in this study we decided to investigate the CO_2 sorption performance of ZIF-300 more deeply with focus on determining the effective synthesis parameters and optimized conditions on CO_2 sorption properties of ZIF-300. The first parameter to be scrutinized is the molar ratio of precursors. The interference of different concentrations of regents into the nucleation and growth processes is one of the key concepts to be perceived [23]. The different rates of nucleation and growth of ZIF-300 crystals directly affect the size of the particles hence the understanding of the pattern and procedure of this phenomenon will be a great asset to control the size and shape of the particles. The second considered parameter is the temperature of the supramolecular assembly process. The reaction temperature as well as concentrations of regents affect the rate of nucleation and growth of ZIF particles [24]. Hence we try to find the quality and quantity of the effect of temperature on the particle sizes. The variation of required time for nucleation and growth is assumed to influence the final size of ZIF-300 nanoparticles. Finally, the effect of three different renowned reaction environments (methanol, DMF and water) for this process will be investigated on the gas sorption capacity of synthesized ZIF-300 particles.

2. Experimental

2.1. Materials

2-methyl Imidazole (99%, meIm), 5(6)-bromobenzimidazole (99%, bmIm), Zinc nitrate hexahydrate (99%, $Zn(NO_3)_2.6H_2O$), Methanol (99.9 % MeOH), Dimethylformamide (99.9%, DMF), Dimethylacetamide (99.9%, DMA), N-Methyl-2-pyrrolidone (99.9%, NMP) and Methanol (99.99%, Methanol) were all purchased from Merck and used as received without further purification.

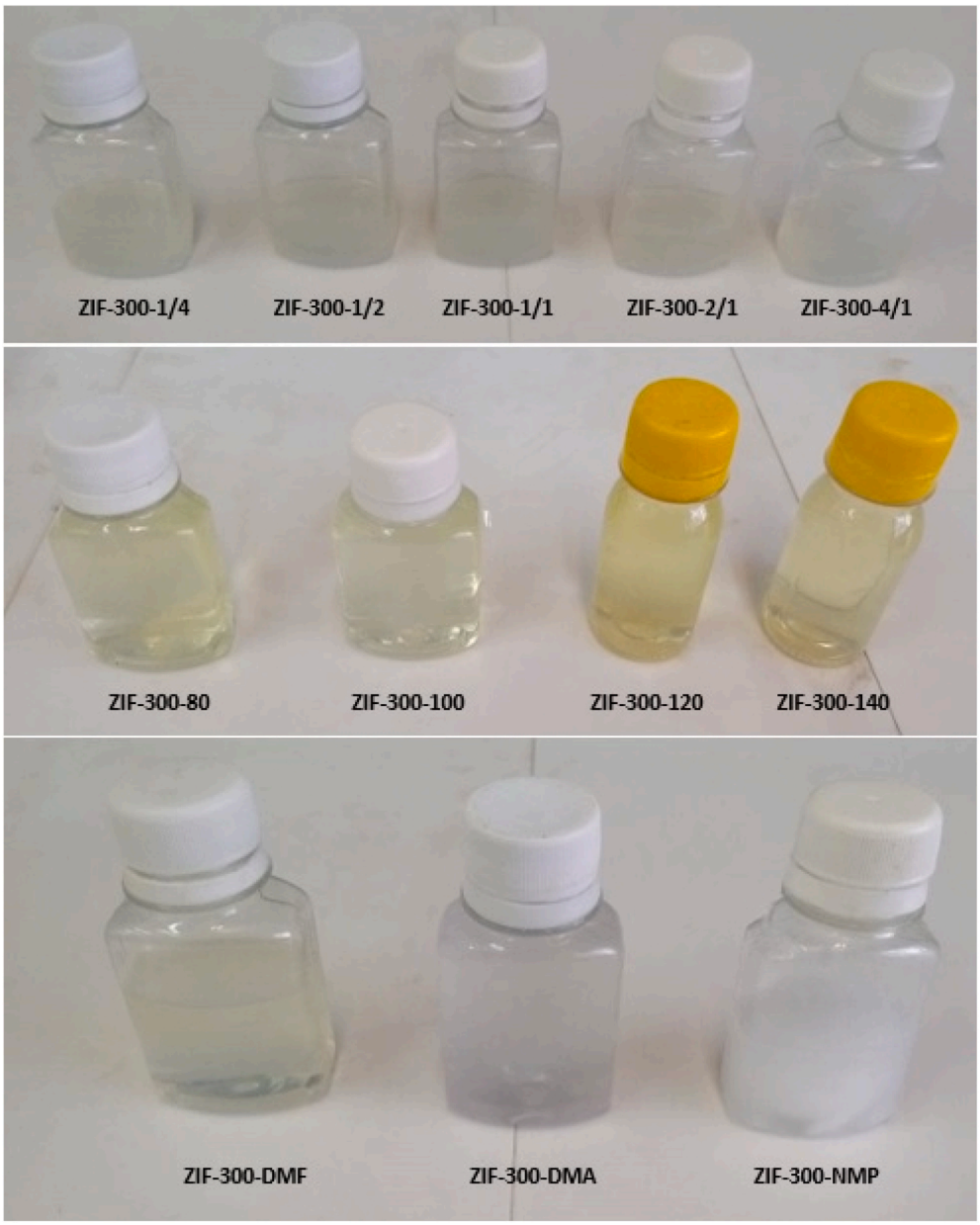

Fig. 2. ZIF-300 samples were prepared with different molar ratios of precursors, at different temperatures and in different mediums.

2.2. Methodology

The ZIF-300 samples were prepared mostly based on a study by the Yaghi group [20] with modifications on molar ratios of precursors, temperature of synthesis environment, and type of solvent used as nucleation and growth environment. Accordingly, 1.43 mmol of bbIm, 1.43 mmol of meIm and 1.14 mmol of $Zn(NO_3)_2.6H_2O$ were each separately dissolved in a mixture of 16 ml of DMF and 1 ml of water at 50 °C for 2 h. Then the resulting three solutions were poured into one capped vial and gently mixed at 120 °C for 72 h on a magnetic stirrer. The resulting turbid solution was then centrifuged for 15 min with the rotation speed of 7000 rpm and then it was washed for 24 h and 5 times, each time with 20 ml of fresh DMF. The resulting as-synthesized ZIF-300 powder was solvent exchanged with methanol 3 times a day for a total duration of three days. The resulting suspension was then centrifuged for 15 min then the methanol was separated from powders. The final step was activation at 180 °C for 2 h to obtain the activated ZIF-300 samples.

Other ZIF-300 samples were produced with the mentioned procedure with modifications only in the temperature of the synthesis environment, amount of utilized bbIm (molar ratio of precursors) and solvents. The abbreviated names of ZIF-300 samples along with details of precursors, the temperature of the synthesis environment and the solvents used are provided in Table 1.

The images of prepared ZIF-300 samples before sedimentation and separation from their solvents are provided in Fig. 2.

As can be seen in this figure there is an obvious difference between the turbidity of samples. The turbidity of samples synthesized with different molar ratios of precursors is different and it can be seen that with the increase in bmim/meIm molar ratio, the turbidity of samples increases meaning that the concentration of synthesized particles is higher in these samples. The samples synthesized at different temperatures do not show noticeable differences in turbidity demonstrating that the concentration of suspended particles in these samples are apparently similar. The difference in turbidity of samples synthesized in different media shows that there is a significant difference between the

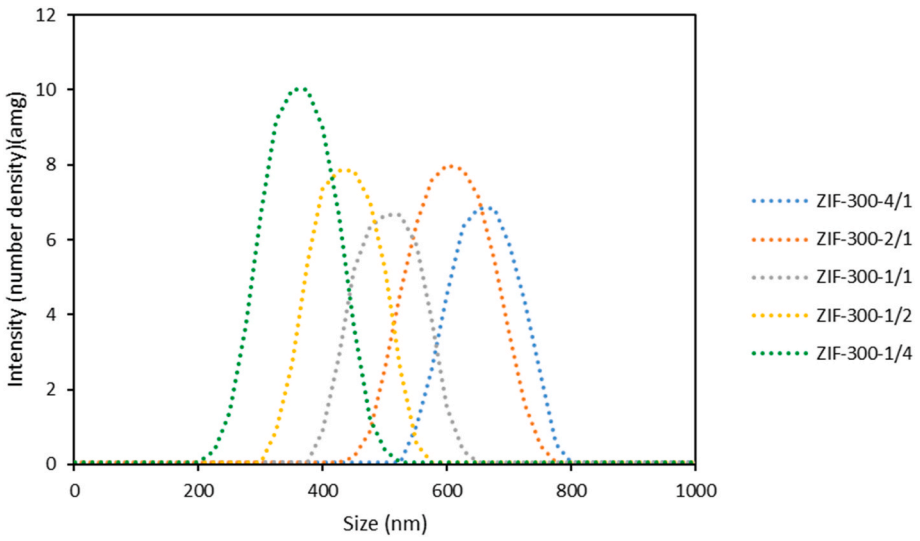

Fig. 3. Particle size distribution (number density vs. size) of ZIF-300 samples prepared with Bmim/meIm molar ratio of (blue) 4/1, (red) 2/1, (grey) 1/1, (yellow) 1/2 and (green) 1/4 in methanol.

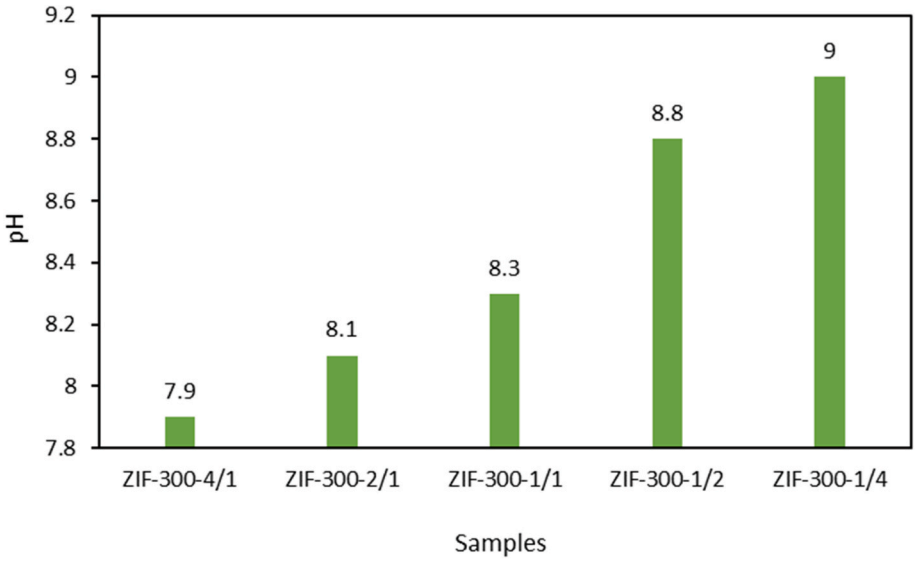

Fig. 4. The ZIF-300 synthesis solution pH as a function of the molar ratio of Bmim/meIm.

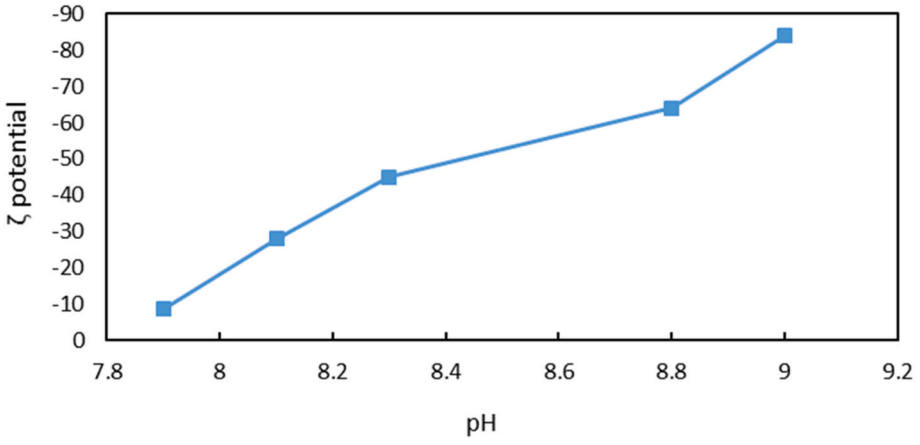

Fig. 5. Zeta potential as a function of pH of synthesis solution.

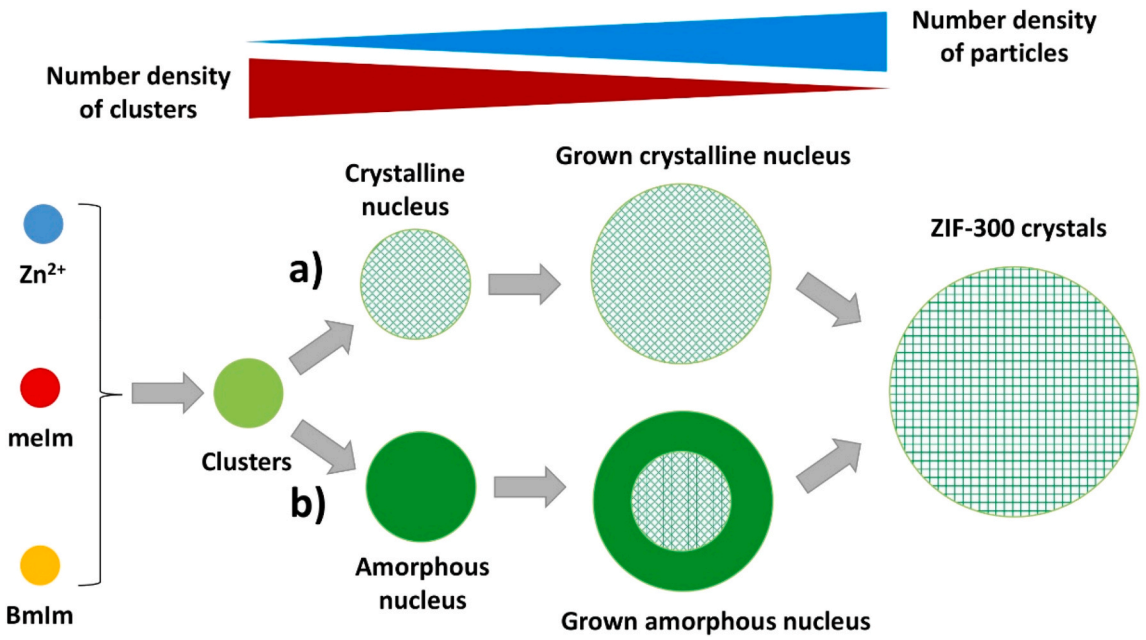

Fig. 6. The procedure of ZIF-300 nanocrystal formation by two different approaches.

concentration or particle size of these samples.

The effect of temperature on the ZIF-300 particle size distribution was studied by preparation of samples by 1:1 M ratio of bmim/meIm, at 80, 100 and 140 °C. The only difference in the synthesis procedure of ZIF-300 is that the temperature of the reaction environment is adjusted by an oil bath at different values. The effect of solvent change on size, shape, crystallinity, specific surface area, sorption capacity and textural properties of samples was studied by synthesis of ZIF-300 separately in DMA and NMP as solvents by the same synthesis procedure.

3. Characterization

The laser particle size analyzer, Zetasizer (Malvern, France) was used to determine the particle size distribution of synthesized ZIF-300 and the value of zeta potentials of particles in the solution. The dried ZIF-300 powder was dispersed in DMF and two successive operations of utilization of a homogenizer and ultrasonic bath were applied each for 30 min to achieve the best possible dispersion of ZIF-300 in the solvent. Scanning Electron Microscopy (SEM) (TESCAN, MIRA3) was applied to visualize the particle size and state of aggregation of synthesized ZIF-300 nanoparticles. An Ion meter (PowerLogic ION8600) was applied for the determination of the pH of the synthesis solutions. X-ray diffraction (XRD) analysis along with gravimetric analysis of the crystallization degree was applied to ensure the synthesis of the ZIF-300 pure phase and to determine the crystallinity of ZIF-300 particles. XRD was performed with Cu Ka radiation (35 kV-35 mA) at step time 2 s and step size of 0.1° by scanning 2θ angle between 1° and 60° using LabX XRD-6100-Shimadzu and the gravimetric analysis was performed using a microbalance (AND GR-300) at different temperatures and several equal periods of times. The H NMR spectroscopy was performed to determine the mole ratios of links in the structure of synthesized ZIF-300 samples. Accordingly, for the preparation of samples, 10 mg of each ZIF-300 sample was placed in a solution consisting of 20 wt% of DCl (0.5 ml) in D_2O and 1 ml of DMF-d_6 and stirred and sonicated successively for 15 min. The gas adsorption capacity of ZIF-300 samples was determined by the N_2 adsorption apparatus (PANAX-PAN-SA2100). About 0.17 g of each ZIF-300 powder was used sample to determine each isotherm at 70 K with an applied vacuum for about 90 min on every sample before the test to empty the occupied pores from possible air molecules. The BET surface area of membranes was calculated based on data from adsorption tests in the pressure range of $0.02<P/P_0<0.2$. The DFT pore size profile of the samples was measured based on density functional theory by specific software provided by the (H-Sorb 2600, Gold APP).

CO_2 and N_2 adsorption analysis for the synthesized ZIF-300 samples was conducted at 25 °C using a volumetric adsorption apparatus (H-Sorb 2600, Gold APP). The pressure range of analysis was adjusted to change between 5 and 100 kPa and before the analysis, the degassing operation of the ZIF-300 samples for removing the residual solvents was conducted by exposing 0.2 g of each sample at 100 °C for 6 h in a degassing chamber.

4. Results and discussion

4.1. Particle size distribution analysis & SEM

The particle size distribution of ZIF-300 samples synthesized with the different Bmim/meIm molar ratios at the temperature of 120 °C has been investigated. In Fig. 3 the particle size distribution of ZIF-300 synthesized with the different molar ratios of precursors is shown versus particle number density (intensity).

From the comparison of different size profiles in Fig. 3 with each other, it can be inferred that, with the decrease in bmim/meIm molar ratio, the peak of the particle size distribution curve moves toward smaller sizes. Accordingly, the number density peak for the sample with the molar ratio of bmim/meIm = 4/1, is at 664 nm whereas this peak for the samples with the molar ratio of Bmim/meIm = 2/1, 1/1, 1/2 and 1/4 is at 610, 522, 417 and 330 nm respectively. This is mainly because the increase in the concentration of meIm ions for the Zn^{2+} creates a barrier of negatively charged meIm ions around the nucleus containing positively charged Zn^{2+} ions [24,25]. This prevents the aggregation of meIm ions around similarly charged ions due to the generated repulsive force. For the interference of bmim, the symmetric structure that was created by meIm ions collapses and this causes the higher possibility of the approach of cations and anions leading to the generation of larger nuclei and finally particles [26,27]. Moreover, there is another consequence of the increase of meIm concentration in the synthesis solution. The increase in meIm concentration will cause an increment in pH of the solution as can be seen in Fig. 4.

According to this figure, the initial pH of the solution increased from 7.9 to 9 as the molar ratio of bmim/meIm decreased from 4/1 to 1/4.

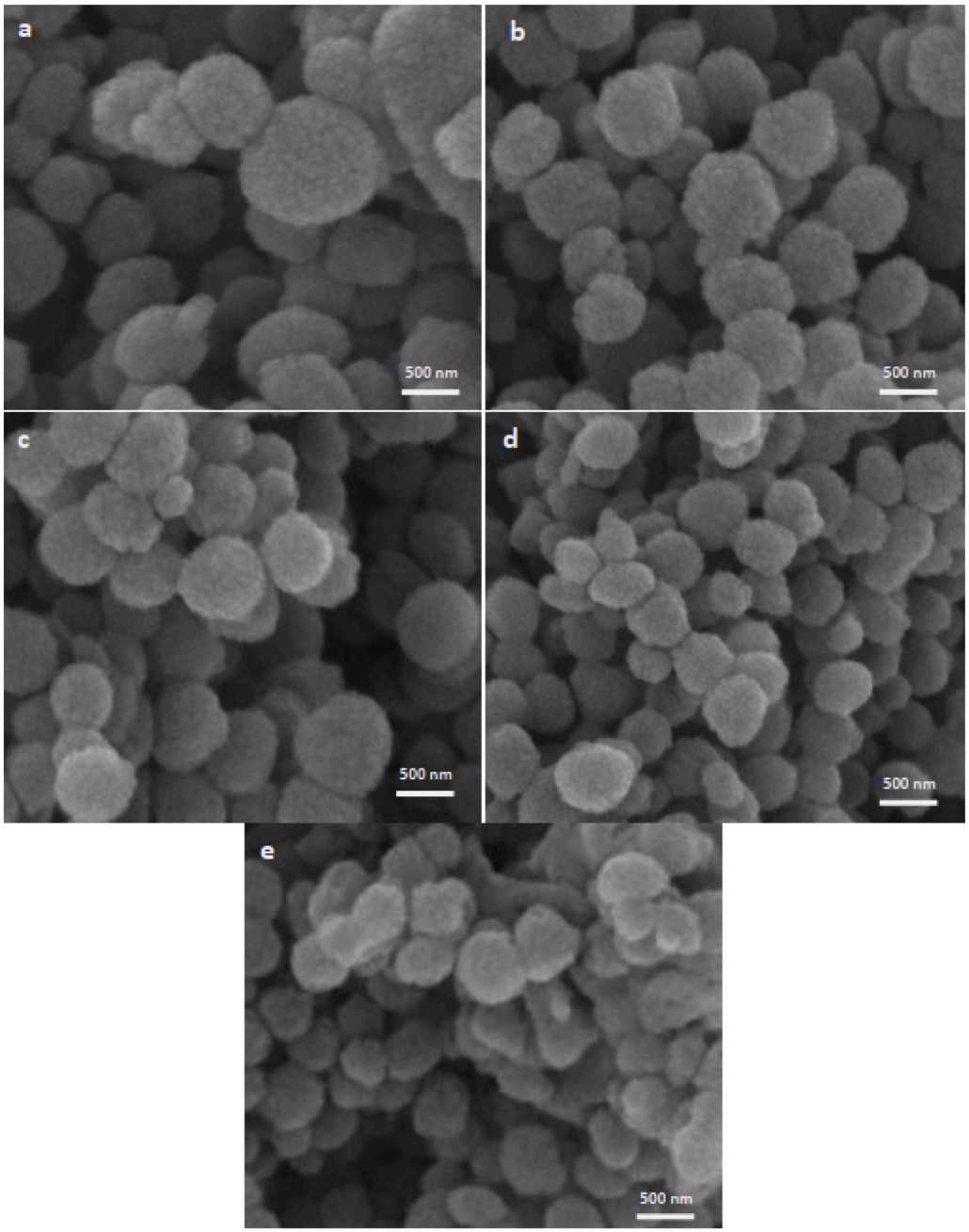

Fig. 7. SEM micrograph of a) ZIF-300-4/1, b) ZIF-300-2/1, c) ZIF-300-1/1, d) ZIF-300-1/2 and e) ZIF-300-1/4.

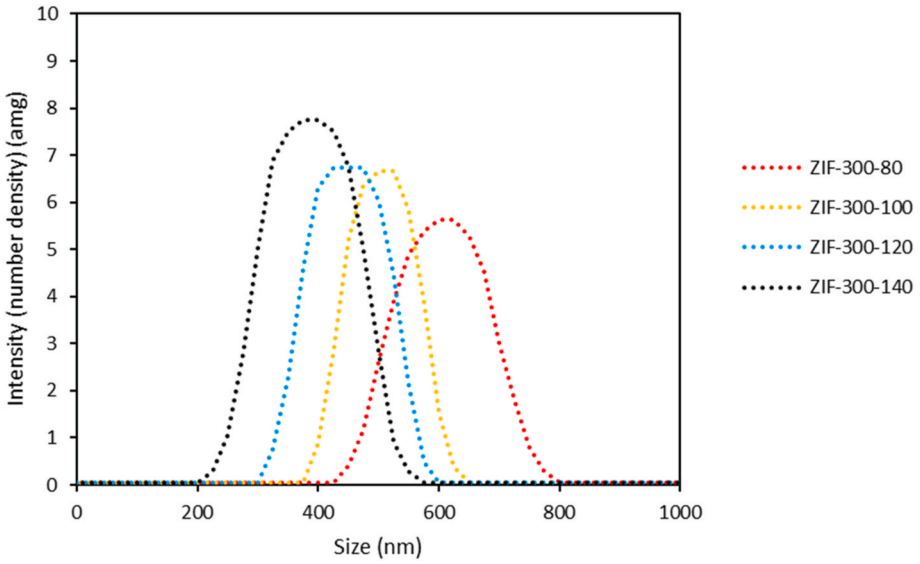

Fig. 8. Particle size distribution (number density vs. size) of ZIF-300 samples prepared at (black) 140 °C, (blue) 120 °C, (yellow) 100 °C and (red) 80 °C.

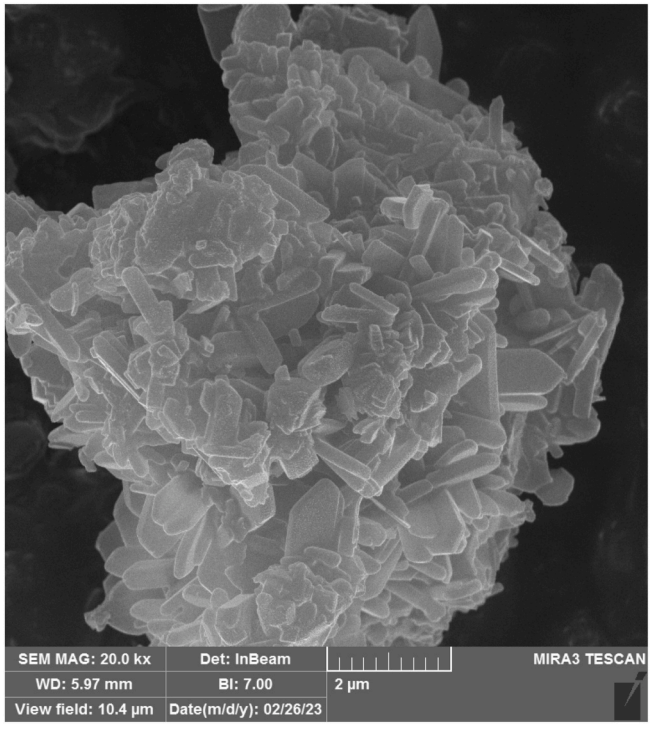

Fig. 9. The SEM image of the overgrown aggregated ZIF-300 particles.

This increase in pH is the reason for the increase in electrostatic repulsive force among negatively charged nuclei or small particles [28,29] which prevents the aggregation of nucleic and particles and also halts the growth of crystals as the zeta potential values of solutions with different pH confirms (Fig. 5).

As can be seen in this figure the increase in pH is accompanied by an increase in zeta potential. The zeta potential is a key indicator of the stability of colloids. Hence it can be said that the larger the zeta potential the higher the degree of electrostatic repulsion between similarly charged particles in the solution which is in agreement with our aforementioned statement.

The reaction between Zn^{2+}, bmim and meIm in the first step leads to the production of clusters which are the seed units before the nucleation process. Then there will be two different possible paths for the formation of ZIF-300 particles [23,30]. The crystal nuclei are born then this nucleus grows to become ZIF-300 nanocrystals. Alternatively, initially, the amorphous nuclei are generated, then these nuclei grow and gradually crystalize and finally transform into ZIF-300 particles (Fig. 6). The required time for the crystallization of nuclei is not clear yet, therefore the determination of the main path of synthesis is not possible. Moreover, it is obvious that the growth of ZIF-300 nanoparticles is a function of the addition of clusters or other smaller species to a larger crystal and it cannot be due to coalescence. This hypothesis seems logical because if the aggregation of particles occurred, the number density of particles had to decrease whereas it increased with time as it is discussed later here in the text.

It is assumed that the growth of particles in a solution is a multi-step process and is directly dependent on the level of supersaturation and surface conditions. According to this, ZIF-300 crystal growth can be divided into several steps and sub-steps. Each sub-step is composed of Angstromic scale growth of nanoparticles and in each of these growth intervals, the accretion of Zn^{2+} and $meIm^{-}$ sub-units are the incentive of growth and not the large clusters or secondary building units. These sub-units build an unenclosed structure in each level which will convert to an enclosed framework in the final step of the growth [24].

The SEM images from the ZIF-300 particles synthesized with different molar ratios of imidazole content are provided in Fig. 7 a-e.

As you can in this figure, the difference between the sizes of ZIF-300 particles is evident. The ZIF-300 particles synthesized with higher bmim/meIm molar ratios have a larger particle size which is in very good agreement with the result of laser PSD analysis.

Fig. 8 represents the particle size distribution of ZIF-300 samples synthesized at different temperatures of 80, 100, 120 and 140 °C.

The comparison of size distributions in Fig. 8 indicates that with the increase in temperature the main peak of distribution moves toward smaller sizes. This observation was an expected outcome because the increase in temperature generally causes a decrease in supersaturation for the materials which has solubility that is directly related to temperature and the decrease in supersaturation will result in the generation of smaller nuclei [31]. As can be seen, the number density of particles synthesized at higher temperatures is noticeably higher than that of particles synthesized at lower temperatures. The reason is related to the fact that when the degree of supersaturation increases (lower temperatures), abundant nuclei are generated due to the existence of a strong driving force of mass transfer from solution to solid state. These nuclei are aggregated to form a larger particle to reduce their energy level and

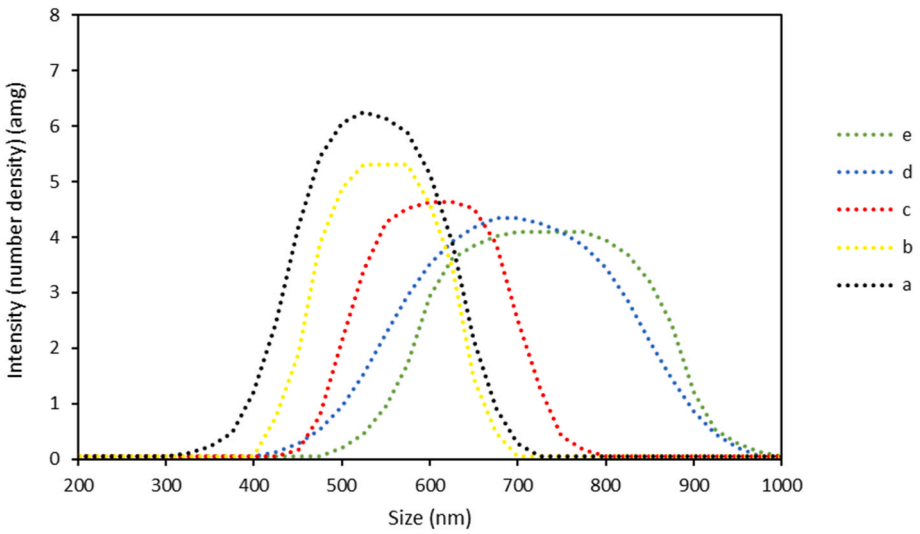

Fig. 10. Particle size distribution (number density vs. size) of ZIF-300 samples prepared at aging time of (a) 3, (b) 6, (c) 12, (d) 24 and (e) 48 h.

reach stability, therefore the number of very small particles and seeds declines. The SEM image of one of the huge particles formed due to the overgrowth and aggregation of particles is presented in Fig. 9. As can be observed, this particle is composed of many smaller particles agglomerated to each other to form this huge structure of ZIF-300 bulk.

The particle size analysis along with SEM Images was also applied to samples synthesized by 1:1 M ratio of bmim/meIm, with different aging times for nucleation and growth. The results of the particle size analysis are presented in Figure (10).

This figure shows that the aging time for nucleation and growth of ZIF-300 particles had a significant effect on the size distribution of these particles. The main peak of particle distribution for samples synthesized with the different allowed aging times of (a) 3, (b) 6, (c) 12, (d) 24 and (e) 48 h are located at 520, 552, 616, 695 and 741 nm respectively. Moreover, the number density of the particles decreases as time passes. This demonstrates that, with the increase in time of nucleation and growth of the particles, not only do the crystals grow larger but also the aggregation of smaller particles as mentioned before, is involved in the creation of larger particles. It is also noteworthy that the mean particle size and number density of particles synthesized at aging times of 24 h and 48 h are very identical. This means that after 24 h of the start of the process, the rate of the growth of particles declines drastically and the driving force of nucleation and growth becomes negligible at this time.

The SEM micrographs of 5 samples fabricated with different aging times are presented in Fig. 11 (a to e).

The results obtained from these SEM images are in good agreement with the results obtained in particle size distribution analysis and it also shows that the aggregation of particles takes part in the creation of larger particles.

The synthesis of ZIF-300 crystals was also performed in DMA and NMP as solvents. The sample with the molar ratio of bmim/meIm = 1/1 was used for both of these environments. Fig. 12 is related to the particle size distribution of the sample synthesized in water.

As can be seen in Fig. 12, the majority of the sizes are around 1000 nm which is much larger than the sizes of ZIF-300 particles synthesized in a DMF environment. The reason is related to the growth and agglomeration of particles as a result of impregnation in a solvent medium which provides lower solubility of precursors. Because of this, the difference between the solubility and current concentration of precursors in the solvent becomes lower. This causes a decrease in supersaturation level and the generation of larger particles. The agglomeration of particles in these two media causes the formation of a very large bulk of ZIF-300 particles with over 2500 nm in size. This means that in DMA and NMP to reach stability, significantly larger particles have to be formed compared with the DMF solution.

The SEM image of a part of synthesized ZIF-300 particles in NMP is presented in Figure (13). As can be seen in this figure the agglomeration of particles is clear and the size of particles is remarkably higher than those synthesized in DMF solution. Furthermore, the shape of the particles does not have sharp edges and clear crystal surfaces which means that the ZIF-300 crystal phase might not be completely formed or it may have some amorphous phases involved.

Fig. 14 shows the deposition of particles in the DMA which is due to the large size and consequently heaviness of ZIF-300 particles.

The SEM micrograph of ZIF-300 particles synthesized in DMA is shown in Fig. 15. The scale of this figure shows that the particle sizes are over 1 μm or more. This micrograph is in very good agreement with the results of the particle size distribution analysis.

4.2. X-ray diffraction and gravimetric analysis

Fig. 16 (a, b and c) shows the X-ray diffraction of ZIF-300 samples prepared with the molar ratio of Bmim/meIm of 1/4, 1/1 and 4/1, respectively.

As it can be seen in this figure, the main peaks from left to right are a reflection of X-rays from crystal planes indicated at angles of 5.5, 6.6, 11.7, 13 and 17.1°. These peaks are in very good agreement with the XRD results of the original work on ZIF-300 reported by the Yaghi group [20]. From the comparison of the spectra of Fig. 16 with each other, we can infer that with the increase in the molar ratio of bmim/meIm, the height of the observable peaks increases as in the molar ratio of 1/1 the intensity of peaks is more than twice higher than that in the molar ratio of 1/4. It can be said that this observation is a result of the increase in the degree of crystallinity of ZIF-300 particles as a result of the increase of bmim/meIm molar ratio and consequently the extension of crystal surfaces in larger particles. The relative crystallinity was determined by analyzing the relative area under the characteristic XRD peaks of ZIF-300 [24].

$$RDC\% = (A/A^*) \times 100 \quad (1)$$

Where, RDC is the relative degree of crystallinity, A is the area under the characteristic peak of a ZIF-300 sample and A* is the maximum area under the characteristic peak of synthesized ZIF-300 samples. This calculation allows for quantification of the crystallinity level of the synthesized ZIF-8 material in comparison to the maximum achievable crystallinity.

However, the increase in the molar ratio of precursor from 1 to 4

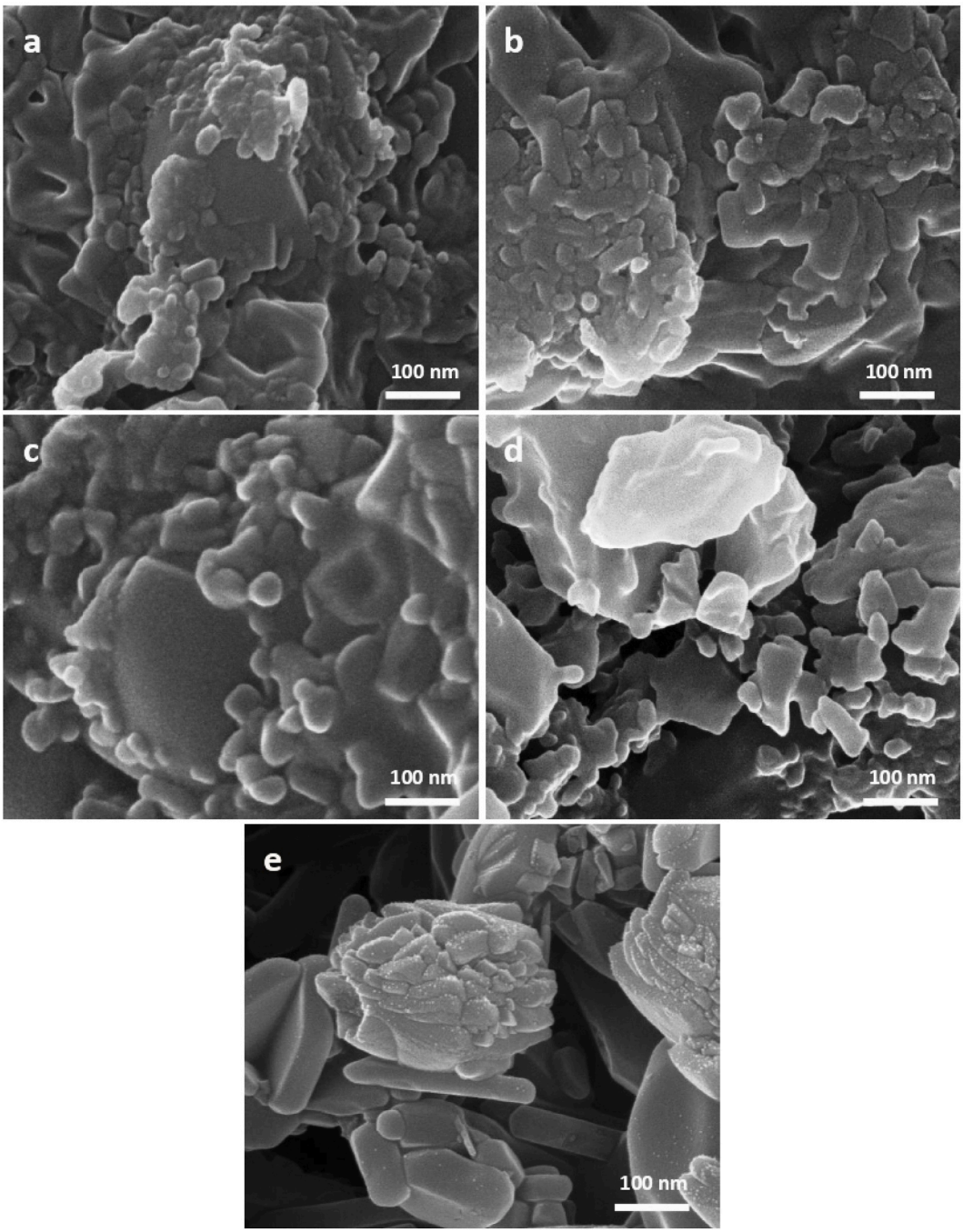

Fig. 11. The SEM image of ZIF-300 samples prepared at the aging time of (a) 3, (b) 6, (c) 12, (d) 24 and (e) 48 h.

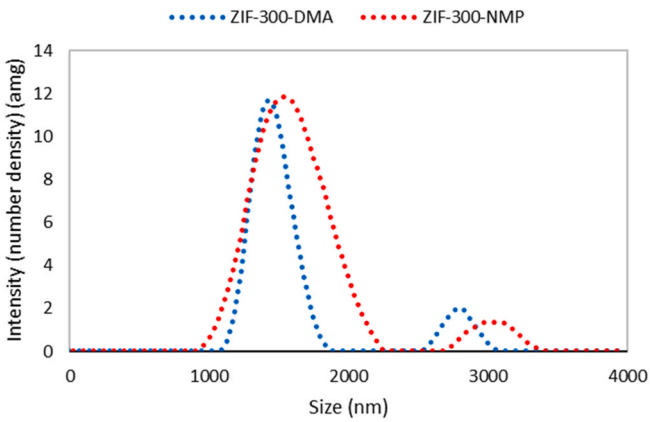

Fig. 12. Particle size distribution (number density vs. size) of ZIF-300 sample prepared with Bmim/meIm molar ratio = 1/1 in DMA and NMP at ambient temperature.

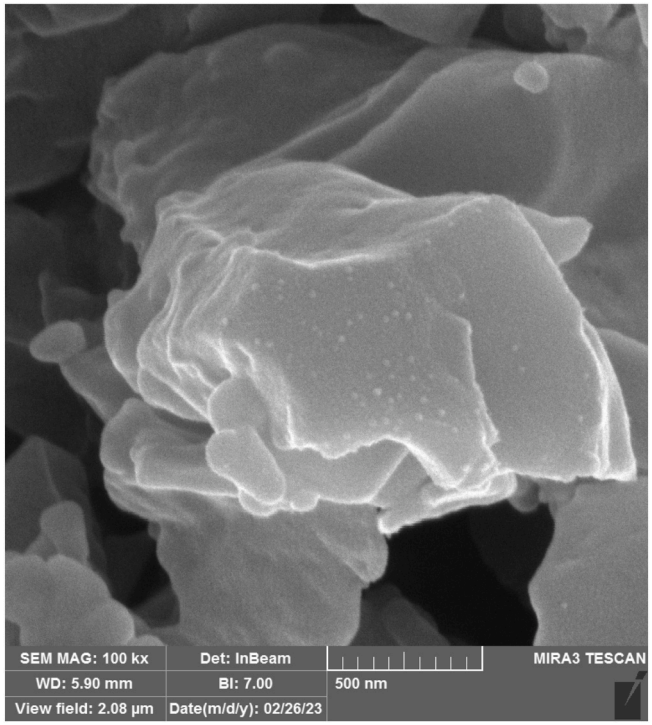

Fig. 13. The SEM image of ZIF-300 particles prepared in the NMP.

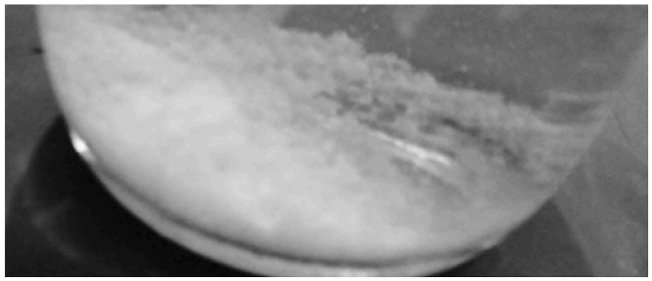

Fig. 14. Micron-sized aggregated particles of ZIF-300 precipitated in the DMA solution.

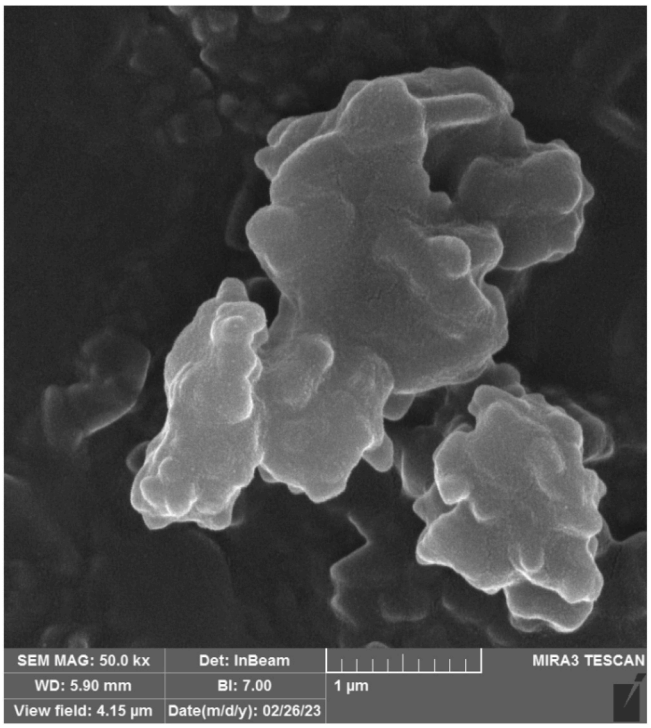

Fig. 15. The SEM images of synthesized ZIF-300 particles in DMA.

does not have a notable impact on the intensity of XRD peaks. The reason seems to be related to the fact that, in the samples synthesized with the molar ratio of precursors = 1/1, after 6 h the degree of crystallinity is high enough (around 88%) that further enhancement in the molar ratio of precursors cannot noticeably exceed it in a few hours. This claim is satisfactorily approved by gravimetric analysis of crystallinity degree as can be seen in Fig. 17.

According to this figure, it can be said that the degree of crystallinity of ZIF-300 particles approaches a constant value at different times. This time is about 120, 240, and 360 min for samples with the molar ratio of bmim/meIm = 4, 2 and higher than 1, respectively. This graph justifies the results from XRD analysis and demonstrates that after a certain period the rate of nucleation and growth of particles decline drastically and after that, the particle size distribution does not change significantly. Moreover, because the crystallinity degree of ZIF-300-4/1sample particles reached almost 100% after about 160 min from the beginning of the synthesis process, it can be concluded that there would be no generation of larger crystals in the synthesis environment with an increase in the molar ratio of bmim/meIm. This means that a further increase in the molar ratio of bmim/meIm may result in the formation of larger agglomerated particles but from the same crystal size of the sample synthesized with the molar ratio of bmim/meIm = 4.

Fig. 18 (a, b, c and d) shows the X-ray diffraction of ZIF-300 samples prepared at 80, 100 and 120 and 140 °C, respectively.

From the comparison of XRD spectra of Fig. 18 with each other, it can be deduced that the intensity of characteristic peaks of ZIF-300 decreased with the increase in temperature. The increase in temperature from 80 to 100 °C had a significant impact on the intensity of peaks however 120–140 °C increase, had a minor impact on the peak's intensity. This can be justified by the fact that the supersaturation level decreases with an increase in temperature and consequently, the degree of crystallinity reduces due to this increase.

The gravimetric analysis of the crystallinity degree of the samples prepared at different temperatures is presented in Fig. 19. As can be seen in this figure, the degree of crystallinity of ZIF-300 particles reduced with increasing temperature. There is a good agreement between the results obtained from this figure with those obtained from XRD analysis.

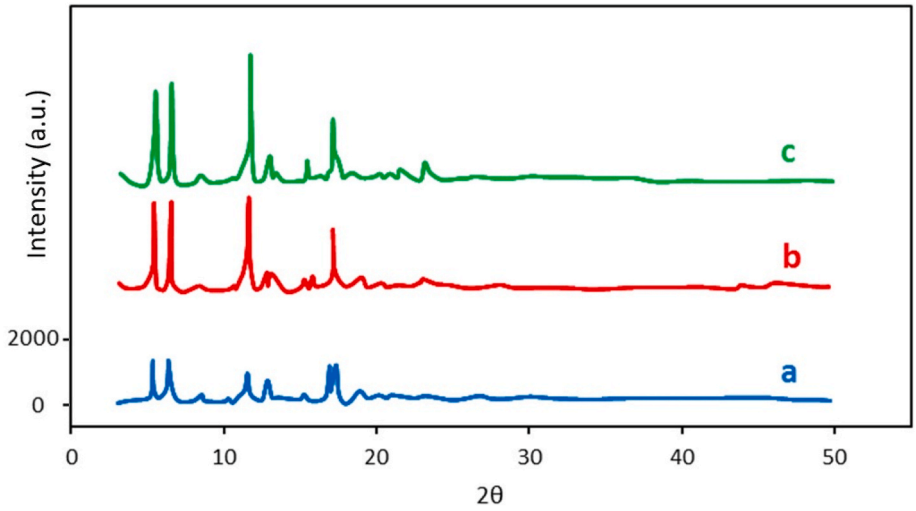

Fig. 16. XRD of ZIF-300 samples synthesized with Bmim/meIm molar ratio of (a) 1/4, (b) 1/1 and (c) 4/1.

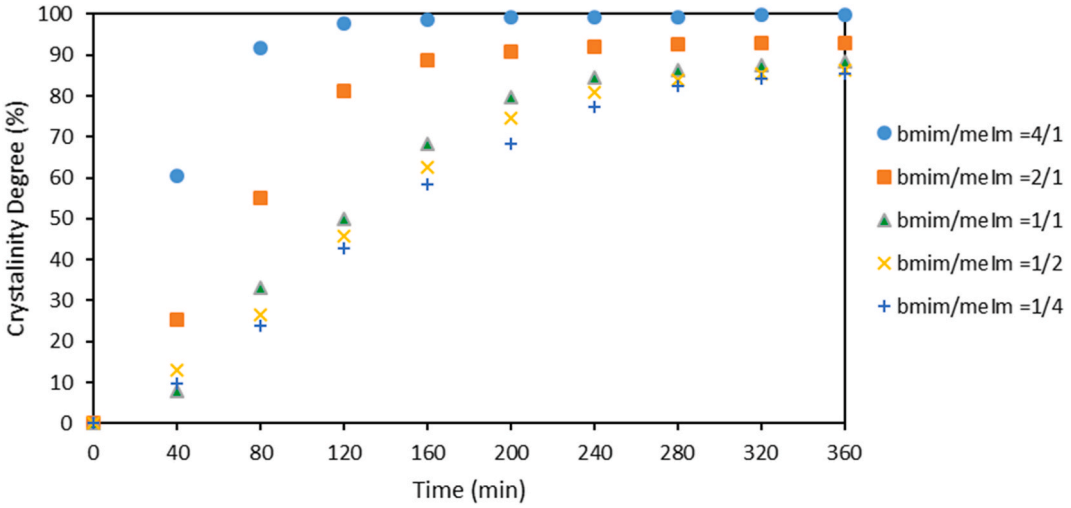

Fig. 17. The crystallinity degree of ZIF-300 samples prepared with the different molar ratios of bmim/meIm versus time.

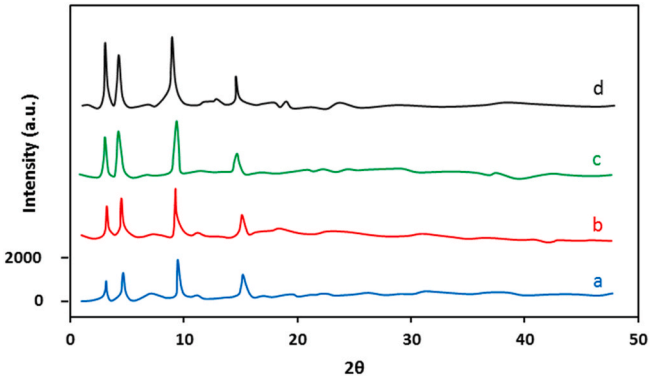

Fig. 18. XRD patterns of ZIF-300 samples synthesized at (a) 140 °C, (b) 120 °C, (c) 100 °C and (d) 80 °C.

As it is clear in this figure, the time required for samples to reach a constant degree of crystallinity, is almost the same for all four samples and it is around 120–140 min, thus, it can be said that the temperature at which samples prepared in, has almost no effect on the time of reaching to a maximum crystallinity degree.

Fig. 20 shows the X-ray diffraction of ZIF-300 samples (bmim/meIm = 1/1) prepared at the aging time of 3, 12, and 48 h, respectively. As this figure shows, the characterization spectra of samples with longer aging time show significantly higher and wider peaks. This is related to the fact that longer aging time results in the creation of larger particles with more stabilized and mature crystal surfaces which better reflect the X-ray [30]. The observation that the sharpness of characteristic peaks of ZIF-300 increases and the peaks become slightly wider as the aging time of sysnthesis increases is in line with the Scherrer equation, which states that peak width is inversely proportional to crystallite size. Larger crystals result in sharper peaks. As ZIF-300 crystals grow and become larger in the synthesis procedure, it is expected that samples subjected to more growth cycles would exhibit wider peaks. This is because the increased crystallite size leads to sharper and more defined peaks in the X-ray diffraction pattern.

4.3. H NMR analysis

Proton nuclear magnetic resonance spectroscopy has been extensively used chemical composition of linkers in MOFs and ZIFs. Fig. 21 a-h presents the H NMR spectra of all different samples synthesized in this work in DMF solvent.

As can be seen in all of the spectra provided in this figure, there are

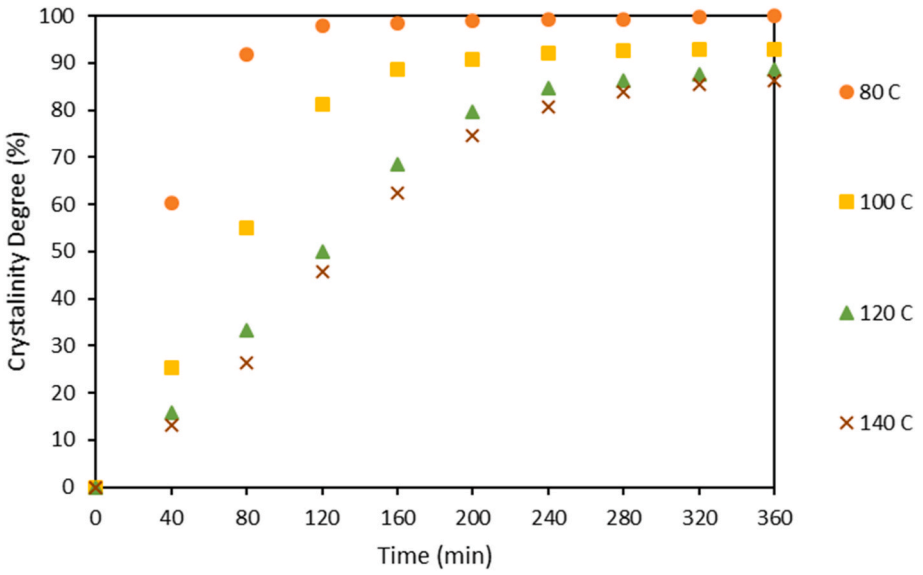

Fig. 19. The crystallinity degree of ZIF-300 samples prepared at different temperatures versus time.

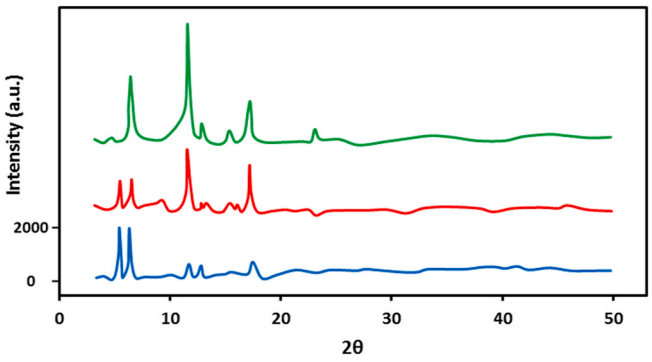

Fig. 20. XRD patterns of ZIF-300 samples synthesized in aging times of (a) 48 h, (b) 12 h and (c) 3 h.

distinct peaks from left to right at chemical shifts of 9.60, 8.02, 7.9, 7.82, 7.72, 7.47, 4.68, 2.84, 2.73 and 2.51. These peaks are respectively related to the hydrogen in methyl group between two nitrogen atoms of imidazole ring (Hd) in bmim, hydrogen in benzene ring adjacent to Br and imidazole ring in bmim molecule (blue Ha), hydrogen in DMF adjacent to C═O, hydrogen in benzene ring adjacent to imidazole ring in bmim molecule (Hc), hydrogen in benzene ring adjacent to Br in bmim molecule (Hb), hydrogen in imidazole ring adjacent to N (red Ha), hydrogen in H_3O^+, hydrogen in CH_3 of DMF, hydrogen in methyl group between two nitrogen atoms of imidazole ring in meIm [20]. In subfigures 20 a-e, which are related to the samples synthesized with the different moral ratio of precursors, as can be seen, with a decrease in the molar ratio of bmim/meIm in the synthesis of ZIF-300 samples, the peaks of hydrogen, related to the bmim in the spectra of the samples become smaller. This is a logical result because the area under each H NMR peak demonstrates the relative abundance of the corresponding hydrogen type in the sample tested. Because the H NMR peaks obtained here are very narrow, the larger the area the higher the height of the peak. The same cannot be said about the hydrogen atoms related to the imidazole ring. This is most probably because 2-methyl imidazole is partly involved in the formation of ZIF-300 structure, hence the meIm molecules in the solution are not the same, hence their hydrogen in the imidazole ring is different, leading to the observation of different corresponding peak heights for these hydrogen atoms.

For the subfigures f-h, which are related to the samples synthesized at different temperatures, as can be seen, no significant difference can be observed between the heights of distinguished peaks in bmim spectra. This is because these samples are synthesized with the same amount and composition of precursors, hence the relative abundance of hydrogen molecules in bmim is nearly the same.

4.4. N_2 adsorption analysis

We also reported the adsorption-desorption isotherms of N_2 in 77 K for ten distinct samples in Fig. 22.

It can be inferred from this figure that the samples prepared in DMF have the highest adsorption capacity for N_2. It seems that NMP and DMA are not the proper solvents for the synthesis of ZIF-300 due to the severe aggregation of particles in these solvents and the generation of huge bulks of particles with lower numbers of exposed pores for adsorption of N_2. With a maximum uptake of 645 cm^3/g the sample prepared in methanol with 4/1 M ratio of bmim/meIm has the highest final uptake among all. The samples synthesized with the larger molar ratio of bmim/meIm have a higher adsorption capacity meanwhile the samples synthesized at lower temperatures have a higher sorption capacity. This is because the higher specific surface area and pore volume originate from the more mature and crystallized structure with a higher degree of crystallinity and larger particle size [23,30]. On the other hand, the smaller particle size causes a higher number of particles in a unit mass of a sample, leading to the achievement of more accessible pores and surface areas. However, because the difference in particle sizes of samples is not huge, this parameter does not have a significant effect on the final sorption capacity of the samples.

It is also noteworthy that the types I and IV of isotherms, which are observed for most of the N_2 adsorption-desorption isotherms are the demonstrations of the presence of micropores and mesopore in the structure of ZIF-300 samples [23]. As can be seen, all of the isotherms show very sharp slopes at very low partial pressures (pressures near zero). This indicates that there are large numbers of mesopores present in the structure of ZIF-300 for all investigated cases. However, the mild slope for some isotherms at higher partial pressures ($0.1<P/P_0<0.9$) indicates the mesopore presence in the structure of particles. Moreover, the hysteresis at medium to high pressures for most of the sample isotherms also demonstrates partial mesoporousity in ZIF-300.

The BET surface area, pore volume and mean pore size of ZIF-300 samples are provided in Table 2.

As can be seen in this table, the BET surface area of samples is

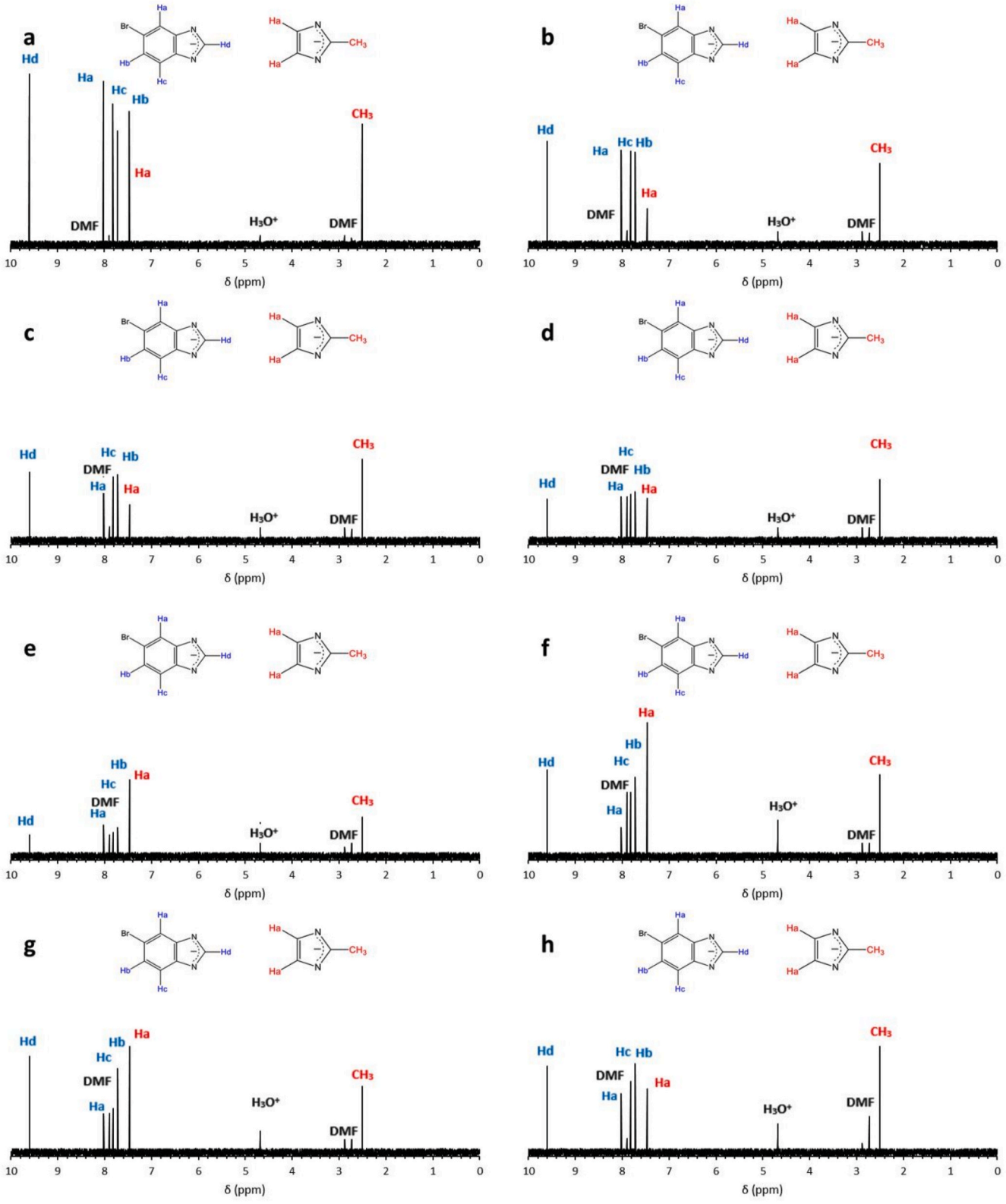

Fig. 21. H NMR spectra of a) ZIF-300-4/1, b) ZIF-300-2/1, c) ZIF-300-1/1, d) ZIF-300-1/2, e) ZIF-300-1/4, f) ZIF-300-80, g) ZIF-300-100 and h) ZIF-300-140.

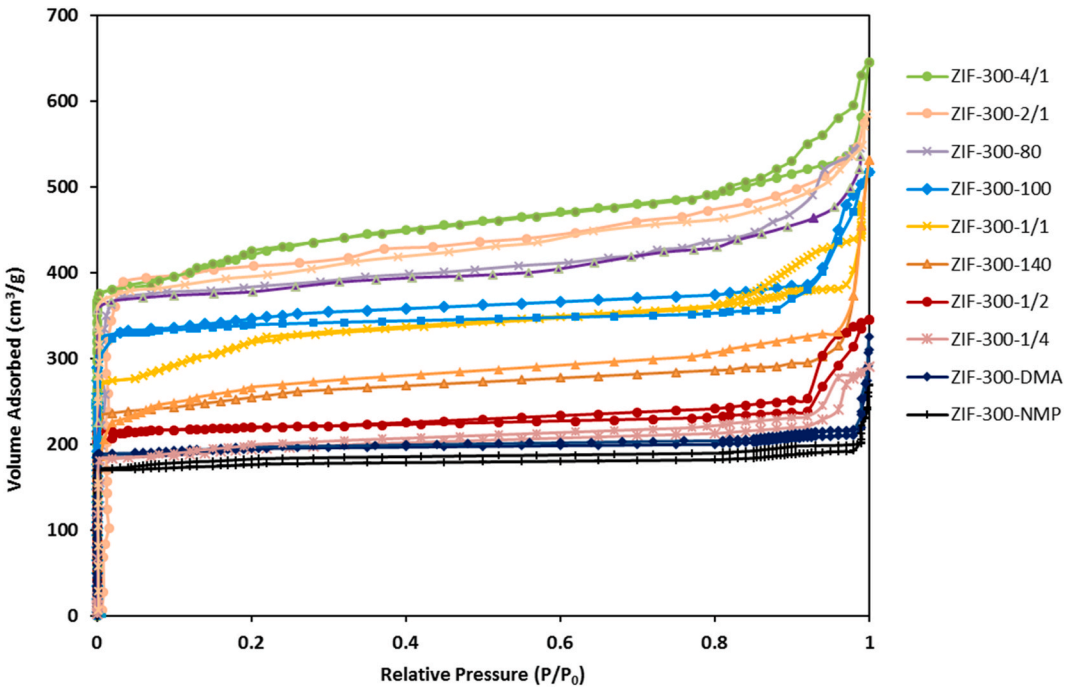

Fig. 22. N_2 adsorption-desorption isotherms of all prepared ZIF-300 samples.

Table 2
Some textural properties of different synthesized ZIF-300 samples.

Sample name	ZIF-300-4/1	ZIF-300-2/1	ZIF-300-80	ZIF-300-100	ZIF-300-1/1	ZIF-300-140	ZIF-300-1/2	ZIF-300-1/4
BET surface area (m^2/g)	610	594	572	551	498	446	432	403
Pore volume (cm^3/g)	0.42	0.40	0.37	0.36	0.33	0.29	0.27	0.24
Mean pore size (nm)	1.88	1.85	1.77	1.75	1.74	1.73	1.70	1.74

between the range of 402–610 m^2/g which is comparable with the value of 546 m^2/g of the work by Yuan et al. [21] The increase in molar ratio of bmim/meIm results in increase in BET surface area of ZIF-300 samples which is in very good agreement with the results of N_2 adsorption-desorption isotherms of samples. These results can be related to the more crystalline structure and formed pores of ZIF-300 samples with the higher molar ratio of bmim/meIm which can be seen in Table 2 as the pore volume of the samples. It is noteworthy that the mean pore size of all the samples is near 2 nm which is significantly larger than the pore size reported by Yuan et al. [21] It appears that the change in the molar ratio of precursors resulted in a notable change in pore size of the samples.

4.5. CO_2/N_2 solubility selectivity

The adsorption isotherms of CO_2 and N_2 at very low pressures ($P < 1$ bar) and at the temperature of 25 °C, for six different ZIF-300 samples are provided in Fig. 23(a–f).

As can be seen in Fig. 23 a-f, the solubility of CO_2 in all synthesized ZIF-300 samples is significantly higher than the solubility of N_2. This demonstrates that all ZIF-300 samples have the potential to be used as adsorbents for CO_2/N_2 separation applications. Moreover, it is also noteworthy that the initial slopes of the CO_2 isotherms are steeper than those obtained for N_2, demonstrating the higher affinity of ZIF-300 samples for CO_2. However, there is a significant difference between the sorption performances of samples. The highest sorption capacity of both CO_2 and N_2 is related to ZIF-300-4/1 and ZIF-300-140 (Fig. 23 a and f). This observation is related to two different reasons. For the case of ZIF-300-4/1, the high sorption capacity is related to the high pore volume and surface area of this sample compared with its counterparts as it was also observed in N_2 adsorption-desorption isotherms. However, for the case of ZIF-300-140, the only explanation for the observation of the high sorption capacity of this sample can be related to the smaller sizes of this sample compared with other synthesized ZIF-300 samples. As it is clear, the number density of a sample with smaller particles is higher than that of a sample with larger particles. This means that there are more numbers of ZIF-300 particles in a unit mass of a sample tested leading to the accessibility of higher surface area and pore volume for gas sorption. This finally results in the observation of higher sorption capacity for this sample. The results of CO_2/N_2 solubility selectivity calculations based on adsorption isotherms are provided in Fig. 24 for six different ZIF-300 samples.

As can be seen in this figure, the highest CO_2/N_2 solubility selectivities are related to the samples synthesized with higher bmim/meIm molar ratio of precursors. Moreover, samples synthesized at lower temperatures show better CO_2/N_2 sorption ability. The highest CO_2/N_2 solubility in different pressures reached 24 which is competitive and slightly higher when compared with the results of original work of Yaghi et al. [20]. It is also worth mentioning that, the CO_2/N_2 solubility of all samples converges when the pressure increases. This is related to the fact that with increase in pressure, the isotherms tend to become more flat and reach a constant value because most of the active pores in ZIF-300 samples are occupied by gas molecules, therefore after a certain pressure, the ration of adsorbed CO_2 and N_2 become constant, and this is

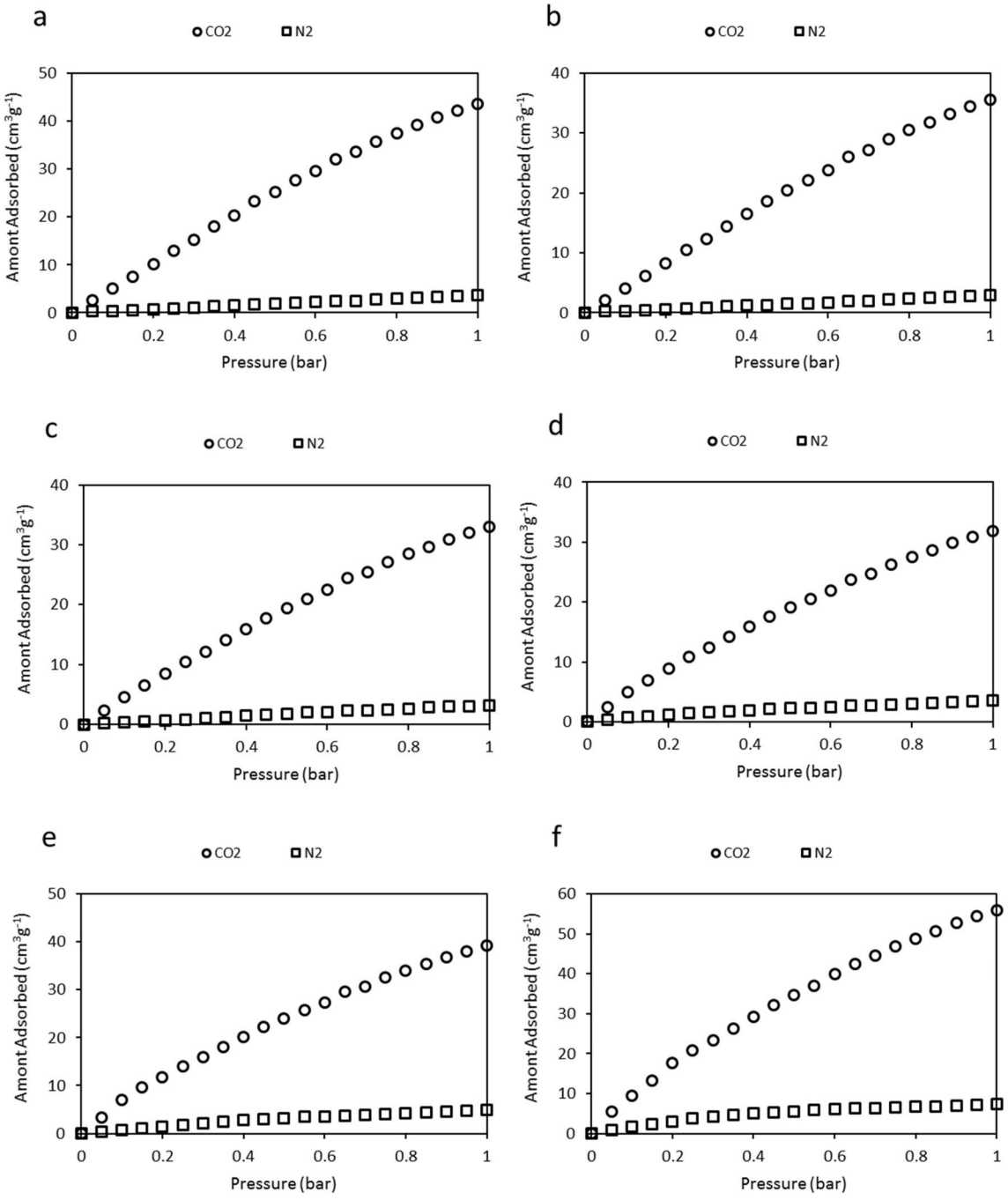

Fig. 23. CO_2 and N_2 adsorption isotherms at low pressures and temperature of 25 °C for a) ZIF-300-4/1, b) ZIF-300-2/1, c) ZIF-300-80, d) ZIF-300-100, e) ZIF-300-1/1 and f) ZIF-300-140 samples.

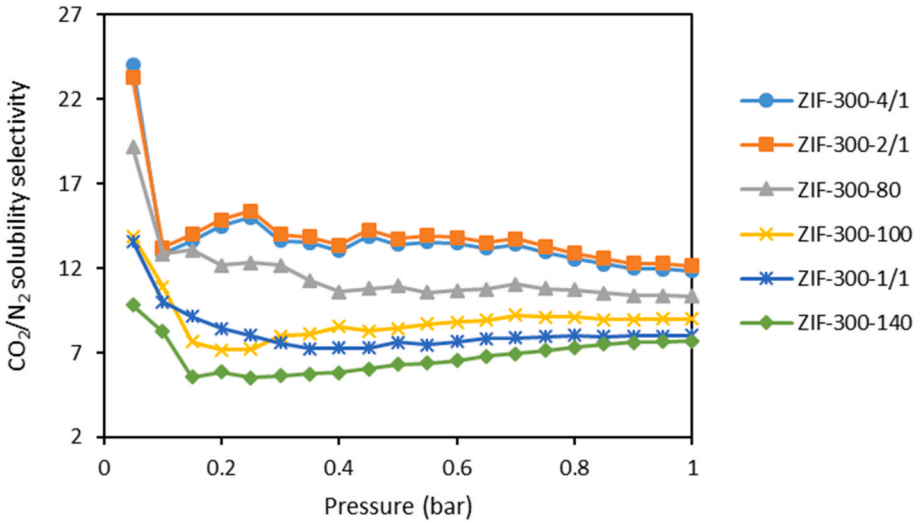

Fig. 24. CO_2/N_2 solubility selectivity for six different ZIF-300 samples at 25 °C and low pressures.

observed for all tested sample cases. The Henry law applied for determination of CO_2/N_2 solubilities at very low pressures, and the result was compared with the work by Yaghi et al. [20] and the work by Yuan et al. [21] in table.

Sample name	ZIF-300-4/1	ZIF-300-2/1	ZIF-300-80	ZIF-300-100	ZIF-300-1/1	ZIF-300-140	ZIF-300 of Yaghi et al. [20]	ZIF-300 of Yaun et al. [21]
CO_2/N_2 solubility	24	23.3	19.2	13.9	13.6	9.8	22	6.4

5. Conclusion

The impact of varying molar ratios of precursors, temperature, time, and synthesis conditions on the crystal structure, textural properties, and CO_2/N_2 sorption behavior of ZIF-300 samples was studied. A higher bmim/meIm molar ratio resulted in larger particle size, increased pore volume, and BET surface area due to a more crystalline and well-defined pore structure. This was attributed to a reduction in the pH of the synthesis solution with higher bmim/meIm molar ratios, leading to decreased zeta potential and less electrostatic repulsion between particles, promoting the formation of larger, more crystalline particles. Elevated synthesis temperatures led to smaller particle formation by reducing supersaturation levels and generating smaller nuclei. Time had a positive effect on particle size due to particle growth and aggregation. NMP and DMA were found to be unsuitable synthesis environments for ZIF-300 samples as they produced large particles with poor gas sorption performance. Samples synthesized with higher bmim/meIm ratios at lower temperatures exhibited superior textural properties, including higher BET surface area and pore volume. Additionally, samples with bmim/meIm molar ratios of 4/1 and 2/1 showed enhanced CO_2/N_2 solubility selectivity compared to other reported cases. It is believed that these ratios of bmim/meIm as it was observed in zeta potential analysis results, caused the formation of more crystalized structure in ZIF-300 particles and therefore more structured pores which resulted in the observation of higher gas adsorption capacity of these powders.

Funding

This research did not receive any specific grant from funding agencies in the public, commercial, or not-for-profit sectors except from Esfarayen University of Technology.

CRediT authorship contribution statement

Abolfazl Jomekian: Writing – original draft, Supervision, Resources, Methodology, Formal analysis, Conceptualization. **Bahamin Bazooyar:** Data curation, Formal analysis, Validation, Writing – review & editing.

Declaration of competing interest

The authors declare that they have no known competing financial interests or personal relationships that could have appeared to influence the work reported in this paper.

Data availability

Data will be made available on request.

References

[1] N. Kannan, D. Vakeesan, Solar energy for future world: - a review, Renew. Sustain. Energy Rev. 62 (2016) 1092–1105, https://doi.org/10.1016/j.rser.2016.05.022.
[2] J.A. Mason, T.M. McDonald, T.H. Bae, J.E. Bachman, K. Sumida, J.J. Dutton, S. S. Kaye, J.R. Long, Application of a high-throughput analyzer in evaluating solid adsorbents for post-combustion carbon capture via multicomponent adsorption of CO2, N2, and H2O, J. Am. Chem. Soc. 137 (2015) 1092–1105, https://doi.org/10.1021/jacs.5b00838.
[3] A. Brunetti, F. Scura, G. Barbieri, E. Drioli, Membrane technologies for CO2 separation, J. Membr. Sci. 359 (2010) 115–125, https://doi.org/10.1016/j.memsci.2009.11.040.
[4] J.C.M. Pires, F.G. Martins, M.C.M. Alvim-Ferraz, M. Simões, Recent developments on carbon capture and storage: an overview, Chem. Eng. Res. Des. 89 (2011) 1446–1460, https://doi.org/10.1016/j.cherd.2011.01.028.
[5] K.K. Wong, Z.A. Jawad, A review and future prospect of polymer blend mixed matrix membrane for CO2 separation, J. Polym. Res. 26 (2019), https://doi.org/10.1007/s10965-019-1978-z.
[6] A.A. Olajire, CO2 capture and separation technologies for end-of-pipe applications - a review, Energy 35 (2010) 2610–2628, https://doi.org/10.1016/j.energy.2010.02.030.
[7] Y.J. Lin, T.H. Pan, D.S.H. Wong, S.S. Jang, Y.W. Chi, C.H. Yeh, Plantwide control of CO2 capture by absorption and stripping using monoethanolamine solution, Ind. Eng. Chem. Res. 50 (2011) 1338–1345, https://doi.org/10.1021/ie100771x.
[8] E. Knapik, P. Kosowski, J. Stopa, Cryogenic liquefaction and separation of CO2 using nitrogen removal unit cold energy, Chem. Eng. Res. Des. 131 (2018) 66–79, https://doi.org/10.1016/j.cherd.2017.12.027.
[9] S.M. Safdarnejad, J.D. Hedengren, L.L. Baxter, Plant-level dynamic optimization of Cryogenic Carbon Capture with conventional and renewable power sources, Appl. Energy 149 (2015) 354–366, https://doi.org/10.1016/j.apenergy.2015.03.100.
[10] D.F. Sanders, Z.P. Smith, R. Guo, L.M. Robeson, J.E. McGrath, D.R. Paul, B. D. Freeman, Energy-efficient polymeric gas separation membranes for a sustainable future: a review, Polymer (Guildf). 54 (2013) 4729–4761, https://doi.org/10.1016/j.polymer.2013.05.075.

[11] P. Yuan, Z. Qiu, J. Liu, Recent enlightening strategies for co2 capture: a review, IOP Conf. Ser. Earth Environ. Sci. (2017) 32–37, https://doi.org/10.1088/1755-1315/64/1/012046.
[12] M.M.H. Shah Buddin, A.L. Ahmad, A review on metal-organic frameworks as filler in mixed matrix membrane: recent strategies to surpass upper bound for CO2 separation, J. CO2 Util. 51 (2021) 101616, https://doi.org/10.1016/j.jcou.2021.101616.
[13] H. Furukawa, K.E. Cordova, M. O'Keeffe, O.M. Yaghi, The chemistry and applications of metal-organic frameworks, Science 341 (2013) 1–6, https://doi.org/10.1126/science.1230444.
[14] J. Zhao, W.W. Dong, Y.P. Wu, Y.N. Wang, C. Wang, D.S. Li, Q.C. Zhang, Two (3,6)-connected porous metal-organic frameworks based on linear trinuclear [Co3(COO)6] and paddlewheel dinuclear [Cu2(COO)4] SBUs: gas adsorption, photocatalytic behaviour, and magnetic properties, J. Mater. Chem. A 3 (2015), https://doi.org/10.1039/c4ta06537a.
[15] J. Zhao, X. Liu, Y. Wu, D.S. Li, Q. Zhang, Surfactants as promising media in the field of metal-organic frameworks, Coord. Chem. Rev. 391 (2019), https://doi.org/10.1016/j.ccr.2019.04.002.
[16] M.M. Yang, J.M. Cao, G.D. Qi, X.Y. Shen, G.Y. Yan, Y. Wang, W.W. Dong, J. Zhao, D.S. Li, Q. Zhang, Construction of low-cost Z-scheme heterojunction Cu2O/PCN-250 photocatalysts simultaneously for the enhanced photoreduction of CO2 to alcohols and photooxidation of water, Inorg. Chem. 62 (2023), https://doi.org/10.1021/acs.inorgchem.3c02026.
[17] A. Jomekian, R.M. Behbahani, Experimental, modeling and AspenPlus simulation of different configurations of membrane separation systems for highly loaded CO2 selective pebax 1657-ZIF-8 membrane, J. Membr. Sci. Res. 7 (2021) 209–223, https://doi.org/10.22079/jmsr.2020.136920.1411.
[18] K.M. Costa Santos, T. dos R. Menezes, C.C. Santana, A. Junges, J. Faccin de Conto, G.R. Borges, C. Dariva, S.M. Egues, E. Franceschi, Study of CO2 and N2 sorption into ZIF-8 at high pressure and different temperatures, J. Solid State Chem. 314 (2022), https://doi.org/10.1016/j.jssc.2022.123370.
[19] R. Banerjee, A. Phan, B. Wang, C. Knobler, H. Furukawa, M. O'Keeffe, O.M. Yaghi, High-throughput synthesis of zeolitic imidazolate frameworks and application to CO2 capture, Science 319 (2008) 939–943, https://doi.org/10.1126/science.1152516.
[20] N.T.T. Nguyen, H. Furukawa, F. Gándara, H.T. Nguyen, K.E. Cordova, O.M. Yaghi, Selective capture of carbon dioxide under humid conditions by hydrophobic chabazite-type zeolitic imidazolate frameworks, Angew. Chem. Int. Ed. 53 (2014) 1–5, https://doi.org/10.1002/anie.201403980.
[21] J. Yuan, H. Zhu, J. Sun, Y. Mao, G. Liu, W. Jin, Novel ZIF-300 mixed-matrix membranes for efficient CO2 capture, ACS Appl. Mater. Interfaces 9 (2017) 38575–38583, https://doi.org/10.1021/acsami.7b12507.
[22] M. Sarfraz, M. Ba-Shammakh, Pursuit of efficient CO2-capture membranes: graphene oxide- and MOF-integrated Ultrason® membranes, Polym. Bull. 75 (2018) 2005–2020, https://doi.org/10.1007/s00289-018-2301-6.
[23] A. Jomekian, B. Bazooyar, R.M. Behbahani, ZIF-8 modified by Pluronic P123 copolymer with enlarged pores and enhanced textural properties for CO2/CH4 and CO2/N2 separations, J. Solid State Chem. 289 (2020) 121532, https://doi.org/10.1016/j.jssc.2020.121532.
[24] A. Jomekian, R.M. Behbahani, T. Mohammadi, A. Kargari, Utilization of Pebax 1657 as structure directing agent in fabrication of ultra-porous ZIF-8, J. Solid State Chem. 235 (2016) 212–216, https://doi.org/10.1016/j.jssc.2016.01.004.
[25] A. Jomekian, B. Bazooyar, R.M. Behbahani, T. Mohammadi, A. Kargari, Ionic liquid-modified Pebax® 1657 membrane filled by ZIF-8 particles for separation of CO2 from CH4, N2 and H2, J. Membr. Sci. 524 (2017) 652–662, https://doi.org/10.1016/j.memsci.2016.11.065.
[26] E. Prouzet, T.J. Pinnavaia, Assembly of mesoporous molecular sieves containing wormhole motifs by a nonionic surfactant pathway: control of pore size by synthesis temperature, Angew Chem. Int. Ed. Engl. 36 (1997) 516–518.
[27] C.-W. Tsai, E.H.G. Langner, The effect of synthesis temperature on the particle size of nano-ZIF-8, Microporous Mesoporous Mater. 221 (2016) 8–13.
[28] M.P. Attfield, P. Cubillas, Crystal growth of nanoporous metal organic frameworks, Dalton Trans. 41 (2012) 3869–3878.
[29] P.Y. Moh, P. Cubillas, M.W. Anderson, M.P. Attfield, Revelation of the molecular assembly of the nanoporous metal organic framework ZIF-8, J. Am. Chem. Soc. 133 (2011) 13304–13307.
[30] A. Jomekian, R.M. Behbahani, T. Mohammadi, A. Kargari, Innovative layer by layer and continuous growth methods for synthesis of ZIF-8 membrane on porous polymeric support using poly (ether-block-amide) as structure directing agent for gas separation, Microporous Mesoporous Mater. 234 (2016) 43–54.
[31] A. Jomekian, R.M. Behbahani, T. Mohammadi, A. Kargari, CO2/CH4 separation by high performance co-casted ZIF-8/Pebax 1657/PES mixed matrix membrane, J. Nat. Gas Sci. Eng. 31 (2016) 562–574, https://doi.org/10.1016/j.jngse.2016.03.067.